



A color-corrected strategy for information multiplexed Fourier ptychographic imaging

Mingqun Wang^{a,b,c}, Yuzhen Zhang^{a,b,*}, Qian Chen^{a,b}, Jiasong Sun^{a,b,c}, Yao Fan^{a,b,c},
Chao Zuo^{a,b,c}

^a School of Electronic and Optical Engineering, Nanjing University of Science and Technology, No. 200 Xiaolingwei Street, Nanjing, Jiangsu Province 210094, China

^b Jiangsu Key Laboratory of Spectral Imaging and Intelligent Sense, Nanjing, Jiangsu Province 210094, China

^c Smart Computational Imaging Laboratory (SCILab), Nanjing University of Science and Technology, Nanjing, Jiangsu Province 210094, China

ARTICLE INFO

Keywords:

Fourier ptychography
Information multiplexing
Color multiplexed fp
LED microscope
Phase retrieval
Biomedical imaging

ABSTRACT

Fourier ptychography (FP) is a novel computational imaging technique that provides both wide field of view (FoV) and high-resolution (HR) imaging capacity for biomedical imaging. Combined with information multiplexing technology, wavelength multiplexed (or color multiplexed) FP imaging can be implemented by lighting up R/G/B LED units simultaneously. Furthermore, a HR image can be recovered at each wavelength from the multiplexed dataset. This enhances the efficiency of data acquisition. However, since the same dataset of intensity measurement is used to recover the HR image at each wavelength, the mean value in each channel would converge to the same value. In this paper, a color correction strategy embedded in the multiplexing FP scheme is demonstrated, which is termed as color corrected wavelength multiplexed Fourier ptychography (CWMFP). Three images captured by turning on a LED array in R/G/B are required as priori knowledge to improve the accuracy of reconstruction in the recovery process. Using the reported technique, the redundancy requirement of information multiplexed FP is reduced. Moreover, the accuracy of reconstruction at each channel is improved with correct color reproduction of the specimen.

© 2017 Elsevier B.V. All rights reserved.

1. Introduction

Fourier ptychographic microscopy (FPM) is a fast-growing computational imaging technique that can overcome the space-bandwidth product limit of a low numerical aperture (NA) imaging system [1]. Both wide-field and high-resolution images of a sample can be obtained without mechanical scanning and interferometric measurements. Owing to its various applications, FPM shows its potential to be used in modern biomedical research, digital pathology, and so on [2].

With similar concept, FPM has developed rapidly with other computational imaging techniques, such as diffractive ptychography and lensfree holographic microscopy [3,4]. Compared with synthetic aperture techniques, FPM has several advantages. Rather than requiring data by mechanical scanning, a programmable LED array substitutes for the original illumination of a microscope to obtain a stack of low-resolution (LR) images of the sample under different illuminating angles. Using the phase retrieval technique, both the HR intensity and the phase information of the object can be resolved with multiple

intensity measurements [5–8]. Besides, as with other computational imaging techniques, aberrations of the optical system can be corrected by implementing the wave-front correction digitally [9,10]. Meanwhile, positional misalignment of the light source could also be corrected by stochastic algorithms, such as simulated annealing method [11–13]. Furthermore, the capacity of high NA imaging has recently been reported, which achieved half-pitch resolution of 154 nm at a wavelength of 435 nm with a 10 \times , 0.4 NA objective lens. This shows further possibilities of label free super resolution imaging [14].

Information multiplexing theory evolved from diffractive ptychography [15–17], which has improved the efficiency of FPM data acquisition. With wavelength multiplexed FP, HR images of samples at R/G/B channels can be recovered by turning on R/G/B LED units simultaneously. Compared with capturing LR images with a monochrome camera at three different wavelengths respectively, the wavelength multiplexed FP reduces the data size by three times. However, since the same dataset is used to recover three HR images at three wavelengths, the mean values

* Corresponding author at: School of Electronic and Optical Engineering, Nanjing University of Science and Technology, No. 200 Xiaolingwei Street, Nanjing, Jiangsu Province 210094, China.

E-mail addresses: wht504066871@163.com (M. Wang), zhangyuzhenjust@163.com (Y. Zhang), surpasszuo@163.com (C. Zuo).

of HR images converge to roughly the same value. In other words, diversity of the samples at different wavelength illuminations is lost in the data acquisition process which will cause a color reproduction problem in recovered result. In digital pathology and biomedical imaging, color information can be very important, particularly in applications such as clinical diagnosis and cell classification.

In this paper, a color correction strategy for multiplexing FP imaging is introduced which requires three additional intensity measurements, while turning on a LED array at each wavelength. These three images can be considered as an incoherent summation of different coherent states. Thus, by bringing these three state multiplexed images into the recovering process and updating the recovered spectrum in Fourier space, the HR image at each channel can be recovered without any resolution (detail) loss. Both simulations and experiments are presented to support the reported scheme. This reported technique, which has been termed color corrected wavelength multiplexed Fourier ptychography (CWMFP), utilizes information multiplexing theory flexibly, which may open up new potential for information multiplexed FP.

2. Methods and simulations

2.1. Forward imaging model of Fourier ptychography

A typical FP microscope is composed of an angle-varied coherent light source (i.e. a programmable LED array or laser source), and a conventional microscope, as shown in Fig. 1(a). The parameters of the system, such as pixel size of imaging sensor and distance between the light source and the object plane affect the overlap ratio $R_{overlap}$ of the pupil in the Fourier plane. The $R_{overlap}$ will further affect the speed and reliability of convergence in reconstruction [18,19]. With the FP concept, the final NA of the system is the sum of illumination and objective NAs, $NA_{eff} = NA_{ill} + NA_{obj}$.

For an imaging system which has a coherent impulse response $h(r)$ and a thin sample $U_o(r)$, where $r = (x, y)$ denotes the lateral coordinates at the sample plane, the imaging process can be described in its simplest form as a convolution operation, $U_i(r) = h(r) * U_o(r)$. In the Fourier plane it can be described as, $G_i(f) = G_o(f) \cdot P(f)$. Where $G_o(f) = \mathcal{F}\{U_o(r)\}$, $\mathcal{F}\{\}$ denotes the Fourier transform operation. $P(f)$ is the pupil function of the imaging system determined by the pixel size of the imaging sensor and cutoff frequency $f_0 = k_0 \cdot NA_{obj}$, which can be considered as a low-pass filter in an imaging system (dashed white circle in Fig. 1(d1) and (d2)), k_0 is the wavenumber at a wavelength of λ . $f = (u, v)$ denotes the coordinates in the Fourier space [20,21].

Assuming a single LED unit illuminates the sample with an oblique plane-wave which has a wave-vector $k_n = (kx_n, ky_n)$, where $n = 1, 2, 3, \dots, N$, N is the total number of units in LED array. The exit light wave from the illuminated sample can be written as $U_e(r) = U_o(r)e^{i(k_n r)}$ and its spectrum $G_e(f - f_n)$ in the Fourier plane has shifted, which means every LED unit corresponding to a specific region in the Fourier space. Therefore, the intensity measurement that the camera captured is

$$I_n(r) = |\mathcal{F}^{-1}\{G_e(f - f_n)P(f)\}|^2. \quad (1)$$

In the case of multiplexing, when the sample is illuminated by multiple LED units, the illumination is normally considered partially coherent. This can be considered as every LED unit at a certain wavelength corresponding to a coherent state. Hence, the multiplexed intensity can be considered as the sum of all states of illumination. For L states of illumination, for example, L monochrome units of LED were turned on every time, the m th multiplexed intensity $I_{L_m}(r)$ can be described as

$$I_{L_m}(r) = \sum_{n \in L} |\mathcal{F}^{-1}\{G_e(f - f_n)P(f)\}|^2, \quad (2)$$

where the set L is chosen from all states of illumination and the symbol \in denotes that n is an element from L .

2.2. Color corrected wavelength multiplexed Fourier ptychography

It is worthwhile reviewing the recovery concept of FP, since the CWMFP is embedded in the information multiplexing FP framework. The basic tool used to recover intensity and phase information was a typical alternating projection (AP) method. That is, solving the phase retrieval problem with known constraints in an iterative manner. In the conventional case of FP, the intensity measurement was set as the constraint in spatial space and the pupil function was the constraint in Fourier space. By applying the constraints in the iterative recovery process, both HR intensity and phase distribution can be restored. Furthermore, with the embedded pupil function recovery technique, pupil function with aberrations can also be restored [22].

Fig. 2 shows a brief scheme of CWMFP. The whole recovery process starts with an initial guess of sample in spatial domain, $U_{\lambda,n}^0 = A_0 e^{i(\varphi_0)}$ (the coordinates were concealed to simplify the equations) where A_0 and φ_0 could be random guesses of the sample, and an initial guess of pupil function $P_{\lambda,n}^0$ which is a binary circle determined by NA of the objective and illumination wavelength λ . In general, a selected initial guess which is close to the ideal image of the sample will further accelerate the recovery. In Fourier domain, the initial guess $O_{\lambda,n}^0$ is the Fourier transform of the initial guess $U_{\lambda,n}^0$, $O_{\lambda,n}^0 = \mathcal{F}\{U_{\lambda,n}^0\}$. In the updating process, assuming the iteration indices $k = 0, 1, 2, \dots, k_{max}$ and the initial guess is set with $k = 0$ and $n = 1$. At k_{th} iteration, a region of the spectrum corresponding to an oblique plane-wave illuminating is inverse Fourier transformed to obtain an estimate of object, $\Psi_{\lambda,n}^k = \mathcal{F}^{-1}\{O_{\lambda,n}^k \cdot P_{\lambda,n}^k\}$. For the conventional FP, the amplitude of $\Psi_{\lambda,n}^k$ is replaced by the square root of intensity measurement whilst retaining the individual phase, $\bar{\Psi}_{\lambda,n}^k = \sqrt{I_{\lambda,n}} \frac{\Psi_{\lambda,n}^k}{|\Psi_{\lambda,n}^k|}$. In the case of multiplexing, the amplitude is replaced by a decomposed amplitude which is created from the integral of each illumination function. Assuming I_{L_m} is the m th intensity measurement under the multiplexing condition, for L states of illumination, it can be described as

$$\bar{\Psi}_n^k = \frac{\sqrt{I_{L_m}}}{\sqrt{\sum_{n \in L} |\Psi_n^k|^2}} \cdot \Psi_n^k. \quad (3)$$

In the case of the wavelength multiplexing, for each wavelength $\lambda = \lambda_1, \lambda_2, \lambda_3$, which corresponds to each wavelength of LED at R/G/B, respectively, the updated estimate can be described as,

$$\bar{\Psi}_{\lambda,n}^k = \frac{\sqrt{I_{L_m}}}{\sqrt{|\Psi_{\lambda_1,n}^k|^2 + |\Psi_{\lambda_2,n}^k|^2 + |\Psi_{\lambda_3,n}^k|^2}} \cdot \Psi_{\lambda,n}^k. \quad (4)$$

Next, The updated spectrum $\bar{O}_{\lambda,n}^k$ can be obtained by transforming the updated estimate $\bar{\Psi}_{\lambda,n}^k$ to the Fourier space and applied pupil constraint, $\bar{O}_{\lambda,n}^k = \mathcal{F}\{\bar{\Psi}_{\lambda,n}^k\} \cdot P_{\lambda,n}^k$. The updated spectrum $\bar{O}_{\lambda,n}^k$ is then used to replace the corresponding region $O_{\lambda,n}^k$ in the Fourier space with the following equations:

$$O_{\lambda,n}^{k+1} = O_{\lambda,n}^k + \alpha \frac{(P_{\lambda,n}^k)^*}{|P_{\lambda,n}^k|_{max}^2} [\bar{O}_{\lambda,n}^k - O_{\lambda,n}^k], \quad (5)$$

$$P_{\lambda,n}^{k+1} = P_{\lambda,n}^k + \beta \frac{(O_{\lambda,n}^k)^*}{|O_{\lambda,n}^k|_{max}^2} [\bar{O}_{\lambda,n}^k - O_{\lambda,n}^k], \quad (6)$$

where $O_{\lambda,n}^{k+1}$ and $P_{\lambda,n}^{k+1}$ are new spectrum and pupil function in the $(k+1)_{th}$ iteration, $O_{\lambda,n}^k$ and $P_{\lambda,n}^k$ are spectrum and pupil function waiting for updating in the k_{th} iteration. α and β are step-size and $*$ denotes the conjugate symbol.

It should be reiterated that $n = 1, 2, 3, \dots, N$ is corresponding to the updating sequence of reconstruction which is determined by illumination NA. That is, a spiral path from inside to outside in the Fourier space. When all regions corresponding to oblique illumination

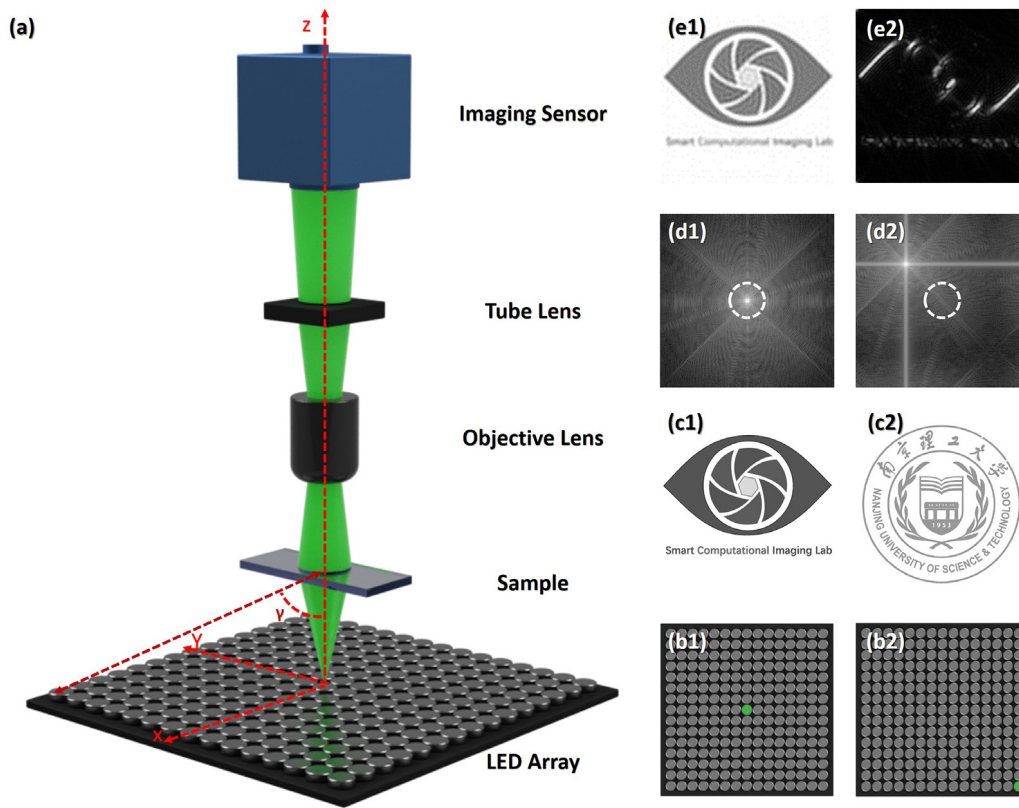


Fig. 1. Conventional FPM platform and imaging process: (a) Basic structure of a FPM system. (b1)–(b2) Lighting unit in LED array. (c1)–(c2) Ideal amplitude and phase of the sample. (d1)–(d2) Oblique illuminated sample in the Fourier space. (e1)–(e2) Bright-field image and dark-field image captured by the imaging sensor.

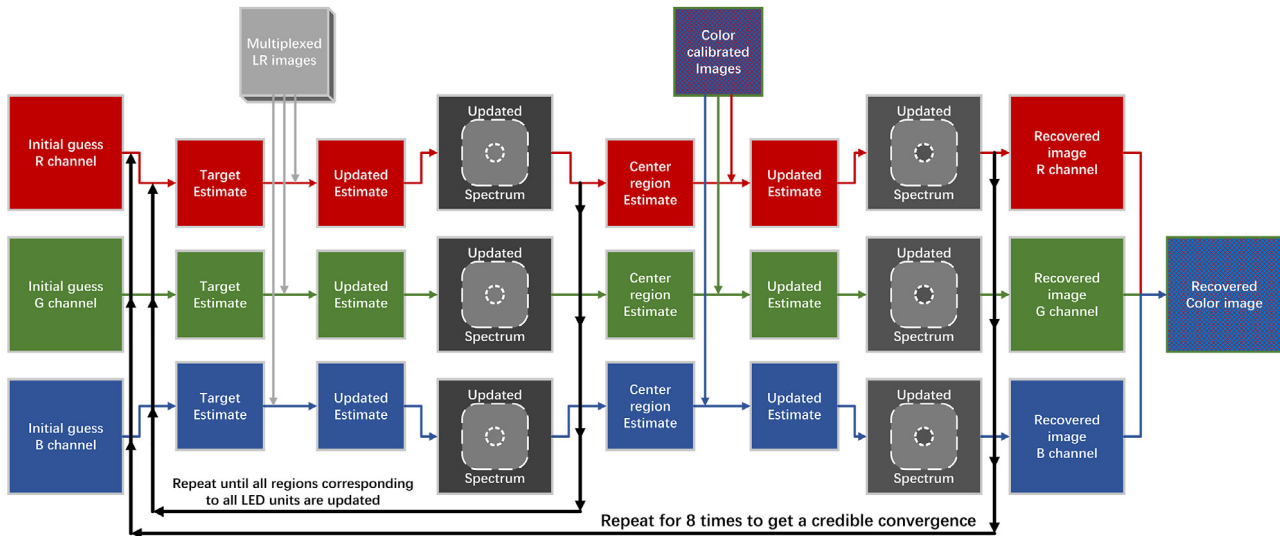


Fig. 2. Flow diagram of CWMFP recovery algorithm.

are updated, the center region of spectrum is updated with a calibrated color image captured by lighting up the LED array which can be done in the data acquisition process. To satisfy Eq. (3), the updated estimate for center region of spectrum $\bar{\Psi}_{\lambda,center}^k$ can be described by

$$\bar{\Psi}_{\lambda,center}^k = \frac{\sqrt{I_{L,\lambda}}}{\sqrt{\sum_{n \in l} |\Psi_{\lambda,n}^k|^2}} \cdot \Psi_{\lambda,center}^k \quad (7)$$

Three images $I_{L,\lambda} = (I_r, I_g, I_b)$ are captured with a low NA objective lens of FP platform by turning on a LED array whose max illumination

NA is smaller than objective lens NA (in this paper a 5×5 LED array is turned on) at R/G/B. The exposure time of camera is adjusted to ensure that these three images have almost the same average intensity value. White balance and gamma correction are then applied to the combined color image to obtain a color corrected image with correct color reproduction of the sample. l is the subset of all illumination states. In this case, since the calibrated color images are captured by turning on a 5×5 array, l is $\{1,2,3, \dots,25\}$ corresponding to all 25 units in the array. The update in the Fourier space follows Eqs. (5) and (6) with the same step-size, $\alpha = \beta = 1$. When the low frequency region is updated,

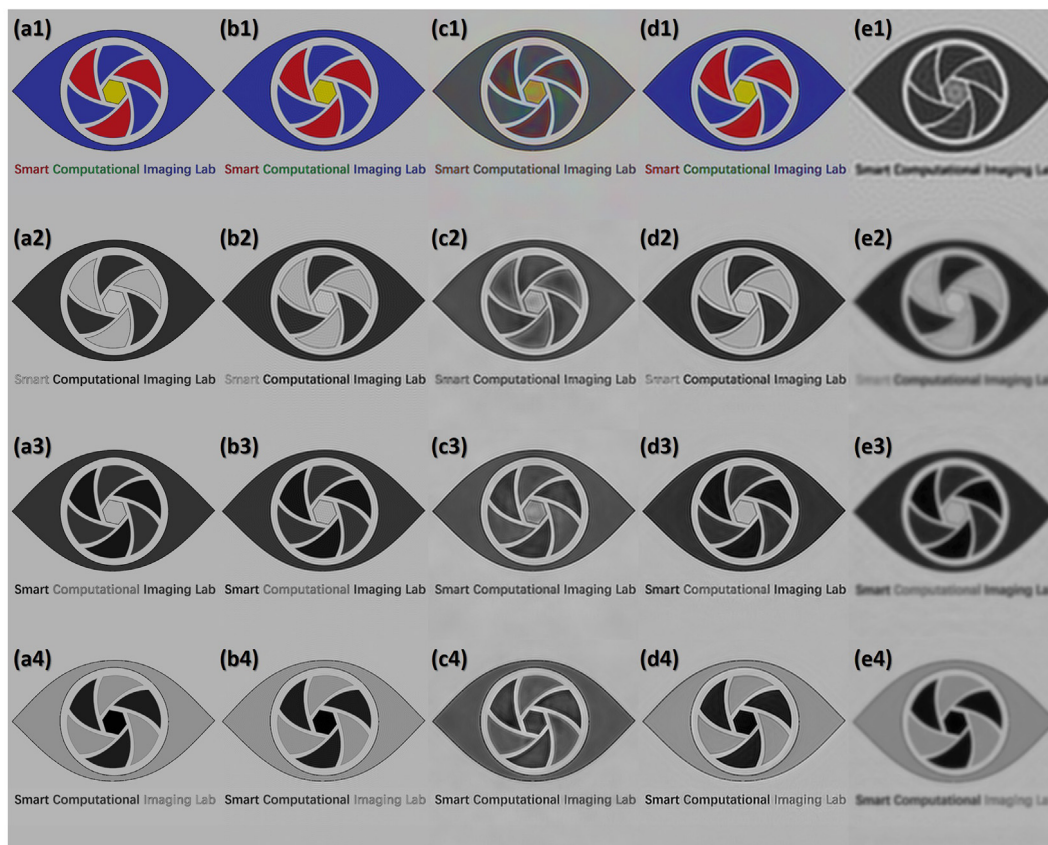


Fig. 3. Simulations of conventional FP, wavelength multiplexed FP and CWMFP. (a1–a4) Ideal input color image and its amplitudes in R/G/B channels. (b1–b4) Recovered HR images with conventional FP. (c1–c4) Reconstructed results of wavelength multiplexed FP (CMFP). (d1–d4) HR images recovered with reported algorithm CWMFP. (e1) Low resolution wavelength multiplexed intensity measurement corresponding to the center LED units. (e2–e4) Low resolution images with turning on a 5×5 array in center of LED array at R/G/B.

a single iteration loop is finished and $k = k + 1$. Then this updated spectrum will play the role of an initial guess and start another recovery iteration. Since the AP method solves the FP problem as a non-convex problem, there is no criterion for the best convergence. In this paper, the maximum number of iteration $k_{max} = 8$.

2.3. Simulations

For validating the performance of CWMFP, the whole imaging process was simulated using MATLAB (Version R2015b, MathWorks, Natick, Massachusetts) on a laptop computer (Intel Core i7-3630MQ 2.40 GHz). The simulation parameters were chosen to be identical to the experiment setup. That is, a 15×15 LED array with exit wavelength of 450 nm, 530 nm, 630 nm, which was placed 42 mm beneath the sample plane. The distance between every LED unit was 1.67 mm. A $4\times$ objective lens was also simulated which has a NA of 0.13 and an imaging sensor with the pixel size of $3.75 \mu\text{m}$. The overlapping-rate (data redundancy) between each aperture in Fourier space $R_{overlap}$ was determined to be $\sim 80\%$, satisfying the convergence condition [18].

The ideal HR amplitude is shown in Fig. 3(a1), Fig. 3(a2–a4) are amplitudes corresponding to R/G/B channels. As a comparison, the conventional FP method was simulated with single state illumination. 225×3 LR images were generated by turning on LED units one by one in R/G/B. The step-size alpha and beta was reduced as $\alpha = \beta = 1, 1/2, 1/3, \dots$ with number of iteration set to 8 to ensure a better convergence. The so called incremental iterative recovery is illustrated in [23], which has been verified to be more robust to noisy data. The reconstructed color image and intensity in R/G/B channels are shown in Fig. 3(b1–b4).

For multiplexed imaging, as previously mentioned, when the sample is illuminated by multiple LED units, the illumination is normally

Table 1
Evaluation of RMSE and mean values at R/G/B channels.

Method	RMSE			Mean		
	R	G	B	R	G	B
FP	0.029	0.021	0.022	0.407	0.388	0.442
CMFP	0.061	0.060	0.076	0.411	0.410	0.412
CWMFP	0.033	0.025	0.026	0.408	0.390	0.444

considered partially coherent, which means every LED unit at a certain wavelength corresponding to a coherent state. In addition, the multiplexed image can be considered as the sum of all states. With this concept, 225 low resolution images were generated as multiplexed images with Eq. (2). Fig. 3(e1) shows the wavelength multiplexed image corresponding to the center units of LED array. The reconstructed HR images with original color multiplexed FP (CMFP) are shown in Fig. 3(c1–c4). It was noted that the diversity of mean values at each channel was not well resolved, as which manifested an incapable color reproduction. Next, three extra images (see Fig. 3(e2–e4)) were generated by turning on a 5×5 LED array in the center of the LED array at R/G/B, respectively. These LR images were put in CWMFP scheme to reconstruct the HR amplitude distribution shown in Fig. 3(d1–d4). The results are close to ideal input images and conventional FP reconstructed images.

The root-mean-square error (RMSE) with the ideal image of the recovered image was introduced to evaluate the quality of reconstruction. From Table 1, it can be seen that, with the original wavelength multiplexed method, the RMSE in each channel is certainly larger since the mean value in corresponding channel converges to a roughly same value. It was also noted that it will be worse if $R_{overlap}$ gets smaller. Under extreme conditions ($R_{overlap} \sim 60\%$ or smaller) the mean values

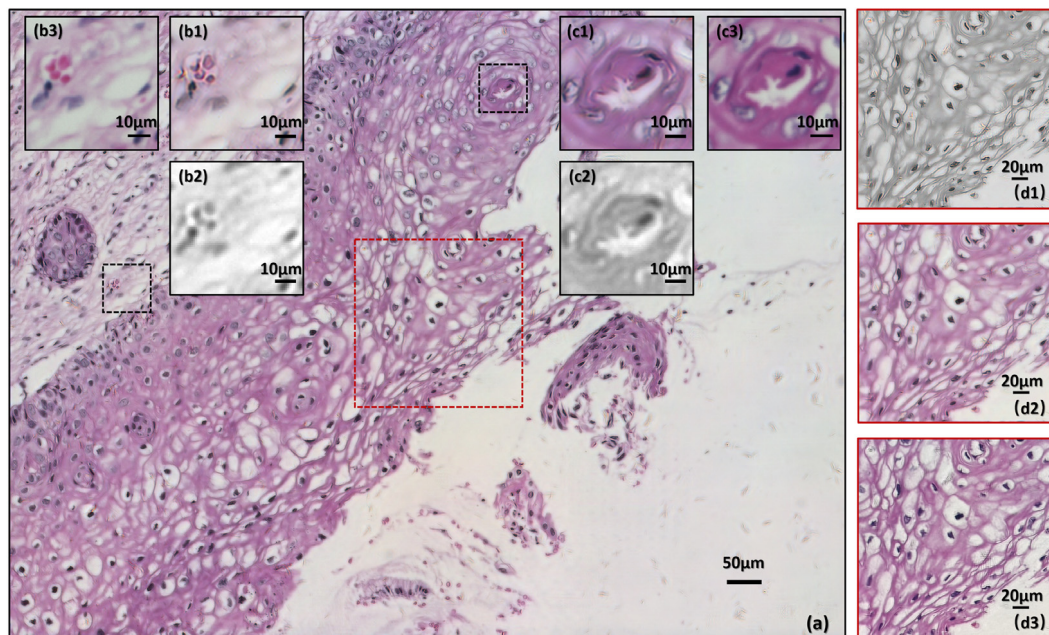


Fig. 4. Experimental results of imaging the pathology slide: (a) Full imaging FoV reconstructed image by the CWMFP. (b1)–(c1) Digitally zoomed area indicated by dashed black box in (a). (b2)–(c2) Wavelength multiplexed raw data. (b3)–(c3) High-resolution image captured with a 10× objective lens (0.4NA). (d1)–(d2)–(d3) Recovered images by the wavelength multiplexed FP, the CWMFP and the conventional FP (without information multiplexing).

will even converge to a same value. This means that increasing data redundancy will effectively support the accuracy of recovery. It is obvious that with a larger mean value error, a larger RMSE results. With the reported CWMFP method, the accuracy of reconstruction at each wavelength can be guaranteed with different $R_{overlap}$ from 60% to 90%, and RMSE in each channel reduces.

3. Experiments and discussions

We validated the CWMFP via real microscope experiment, with the same parameters as in the simulations. The LR images were recorded by a monochrome CCD sensor (Imaging Source DMK 23U445, 1280 × 960 pixels, pixel size 3.75 μm, imaging FoV ~ 1 mm²), the experimental samples were carefully chosen to meet the requirement of the thin object approximation. A 4× objective lens with NA = 0.13 (Olympus UPlan) provided less aberrated raw data for reconstruction. The 15 × 15 LED array was set at 42 mm below the sample plane which had a maximum illuminating NA of ~ 0.27. The total NA of imaging system can be determined as ~ 0.40. Brightness calibration was first implemented to correct the brightness error of LED units. The relative coefficient was calculated from the measured normalized brightness of the LED unit to adjust the LR intensity measurement. Then background noise of raw intensity images was removed.

Brightness calibration and noise removal are important preprocessing procedures for FP imaging. The LED array in the FP platform consistently suffered from the irradiation non-uniformity of the LED units, which greatly affects the reconstruction quality [10]. Furthermore, this illumination error changes with such factors as the distance between the LED array and the sample, and the working time of the LED units. In this work, the calibration procedure was carried out before the data acquisition process. First, a high NA objective lens was used, which has a larger NA than illumination NA to capture a stack of LR images. All LR images corresponding to every LED units in LED array are bright-field images $I_{(n,R)}$, $I_{(n,G)}$, $I_{(n,B)}$. Next, the mean intensities of these images were calculated and the normalized illumination brightness $C_{(n,R)}$, $C_{(n,G)}$, $C_{(n,B)}$ at each channel could be obtained. These normalized parameters will be used to compensate the non-uniformity of the LED units before the iterative recovery procedure of the FP.

The raw data recorded by the camera always suffered from noise, which is normally considered as Poisson noise and white Gaussian noise [24,25]. Especially for dark-field images, the signal noise ratio (SNR) has a conspicuous falloff with camera noise, since the high-frequency (detail) information can be easily covered by the noise. That is a reason why the measured resolution was worse than theoretical resolution each time. Using a camera with better SNR, extending exposure time of the camera and increasing the power of the illuminator are effective ways to improve the final performance of a FP platform. Although, many computational strategies are proposed to improve robustness of FP recovery, at present, the most efficient way to improve the reconstruction quality without replacing the hardware is to set a threshold value in the LR dark-field images to remove background noise. This can be obtained by calculating a mean value of background area in the observed sample. After these preprocess procedures, the modified data can be put into the recovery scheme to recover the HR images.

The experimental results of imaging a pathology slide are shown in Fig. 4. A stained human cervical cancer slide was chosen as the sample. Fig. 4(a) is the full FoV HR image of reconstruction, with Fig. 4(b1) and (c1) showing the digital zoomed in area in Fig. 4(a). Fig. 4(b2) and (c2) display raw multiplexed images. Fig. 4(b3) and (c3) are combined color images captured with a 10× objective lens (Olympus UPlanSApo 0.4 NA). Another comparison of original color multiplexed FP, CWMFP and conventional FP is shown in Fig. 4(d1–d3), where Fig. 4(d1) is the HR RGB image recovered by the original color multiplexed FP, Fig. 4(d2) is a HR RGB image recovered by the reported technique while Fig. 4(d3) is the same region obtained by conventional FP (without information multiplexing). As can be seen, the original color multiplexed FP image has lost the color information of the object. The difference of mean intensity at each channel could not be resolved. Using the reported method, a HR color image with good agreement in both color and details with a conventional microscope image and conventional FP image was obtained.

4. Conclusion

The information multiplexing technique has much enhanced the efficiency of FP data acquisition, which has introduced a novel strategy for multi-spectral microscopy imaging. In this paper, an improved

wavelength multiplexed FP, CWMFP, which improves the accuracy of reconstruction at each wavelength was reported. While high data redundancy is required for information multiplexed FP, multiple LED illumination can provide higher power illumination which can reduce the exposure time of the imaging sensor and improve SNR of any captured dark-field images. However, how to recover the diversity at each channel without any priori knowledge is a significant problem. It is also noted that this reported method can be further developed to implement multiple modes of multiplexed FP. Multiple LED units with white illumination can be turned on simultaneously and the size of FP dataset can be further reduced. Furthermore, more accurate color reproduction of the sample can be obtained by calibrating the color of calibrated images in color space more precisely [26]. Overall, Information multiplexing technique has much potential and should be investigated further.

Acknowledgment

C. Zuo thanks the support of the ‘Zijin Star’ program of Nanjing University of Science and Technology.

Funding information

This work was supported by the National Natural Science Fund of China (61505081, 111574152), Final Assembly “13th Five-Year Plan” Advanced Research Project of China (30102070102), National Key Technologies R&D Program of China (2017YFF0106400, 2017YFF0106403), Six Talent Peaks project of Jiangsu Province, China (2015-DZXX-009), 333 Engineering Research Project of Jiangsu Province, China (BRA2016407, BRA2015294), Fundamental Research Funds for the Central Universities (30917011204, 30916011322), Open Research Fund of Jiangsu Key Laboratory of Spectral Imaging & Intelligent Sense (3091601410414).

References

- [1] G. Zheng, R. Horstmeyer, C. Yang, Wide-field, high-resolution Fourier ptychographic microscopy, *Nat. Photon.* 7 (9) (2013) 739–745.
- [2] G. Zheng, Breakthroughs in photonics 2013: Fourier ptychographic imaging, *IEEE Photon. J.* 6 (2) (2014) 1–7.
- [3] A. Greenbaum, W. Luo, T.-W. Su, Z. Göröcs, L. Xue, S.O. Isikman, A.F. Coskun, O. Mudanyali, A. Ozcan, Imaging without lenses: achievements and remaining challenges of wide-field on-chip microscopy, *Nat. Methods* 9 (9) (2012) 889–895.
- [4] J. Rodenburg, Ptychography and related diffractive imaging methods, *Advances in Imaging and Electron Physics* 150 (2008) 87–184.
- [5] J.R. Fienup, Phase retrieval algorithms: a comparison, *Appl. Opt.* 21 (15) (1982) 2758–2769.
- [6] R.W. Gerchberg, A practical algorithm for the determination of the phase from image and diffraction plane pictures, *Optik* 35 (1972) 237–246.
- [7] R. Horstmeyer, R.Y. Chen, X. Ou, B. Ames, J.A. Tropp, C. Yang, Solving ptychography with a convex relaxation, *New J. Phys.* 17 (5) (2015) 053044.
- [8] L.-H. Yeh, J. Dong, J. Zhong, L. Tian, M. Chen, G. Tang, M. Soltanolkotabi, L. Waller, Experimental robustness of Fourier ptychography phase retrieval algorithms, *Opt. Express* 23 (26) (2015) 33214–33240.
- [9] P. Thibault, M. Dierolf, O. Bunk, A. Menzel, F. Pfeiffer, Probe retrieval in ptychographic coherent diffractive imaging, *Ultramicroscopy* 109 (4) (2009) 338–343.
- [10] Z. Bian, S. Dong, G. Zheng, Adaptive system correction for robust Fourier ptychographic imaging, *Opt. Express* 21 (26) (2013) 32400–32410.
- [11] J. Sun, Q. Chen, Y. Zhang, C. Zuo, Efficient positional misalignment correction method for Fourier ptychographic microscopy, *Biomed. Opt. Express* 7 (4) (2016) 1336–1350.
- [12] A. Maiden, M. Humphry, M. Sarahan, B. Kraus, J. Rodenburg, An annealing algorithm to correct positioning errors in ptychography, *Ultramicroscopy* 120 (2012) 64–72.
- [13] L. Bian, G. Zheng, K. Guo, J. Suo, C. Yang, F. Chen, Q. Dai, Motion-corrected Fourier ptychography, *Biomed. Opt. Express* 7 (11) (2016) 4543–4553.
- [14] J. Sun, C. Zuo, L. Zhang, Q. Chen, Resolution-enhanced Fourier ptychographic microscopy based on high-numerical-aperture illuminations, *Sci. Rep.* 7 (1) (2017) 1187.
- [15] S. Dong, R. Shiradkar, P. Nanda, G. Zheng, Spectral multiplexing and coherent-state decomposition in Fourier ptychographic imaging, *Biomed. Opt. Express* 5 (6) (2014) 1757–1767.
- [16] D.J. Batey, D. Claus, J.M. Rodenburg, Information multiplexing in ptychography, *Ultramicroscopy* 138 (2014) 13–21.
- [17] L. Tian, X. Li, K. Ramchandran, L. Waller, Multiplexed coded illumination for Fourier ptychography with an LED array microscope, *Biomed. Opt. Express* 5 (7) (2014) 2376–2389.
- [18] J. Sun, Q. Chen, Y. Zhang, C. Zuo, Sampling criteria for Fourier ptychographic microscopy in object space and frequency space, *Opt. Express* 24 (14) (2016) 15765–15781.
- [19] S. Dong, Z. Bian, R. Shiradkar, G. Zheng, Sparsely sampled Fourier ptychography, *Opt. Express* 22 (5) (2014) 5455–5464.
- [20] D.G. Voelz, *Computational fourier optics: a MATLAB tutorial*, SPIE press Bellingham, WA, 2011.
- [21] G. Zheng, *Fourier ptychographic imaging: a MATLAB tutorial*, Morgan & Claypool Publishers, 2016.
- [22] X. Ou, G. Zheng, C. Yang, Embedded pupil function recovery for Fourier ptychographic microscopy, *Opt. Express* 22 (5) (2014) 4960–4972.
- [23] C. Zuo, J. Sun, Q. Chen, Adaptive step-size strategy for noise-robust Fourier ptychographic microscopy, *Opt. Express* 24 (18) (2016) 20724–20744.
- [24] Y. Zhang, P. Song, Q. Dai, Fourier ptychographic microscopy using a generalized anscombe transform approximation of the mixed Poisson–Gaussian likelihood, *Opt. Express* 25 (1) (2017) 168–179.
- [25] Y. Fan, J. Sun, Q. Chen, M. Wang, C. Zuo, Adaptive denoising method for Fourier ptychographic microscopy, *Opt. Commun.* (2017).
- [26] Y. Zhang, Y. Wu, Y. Zhang, A. Ozcan, Color calibration and fusion of lens-free and mobile-phone microscopy images for high-resolution and accurate color reproduction, *Sci. Rep.* 6 (2016) 27811.